X-621-74-246
PREPRINT

NASA TM X- 70748

THE GLOBAL CHARACTERISTICS OF ATMOSPHERIC EMISSIONS IN THE LOWER THERMOSPHERE AND THEIR AERONOMIC IMPLICATIONS

(NASA-TM-X-70748) THE GLOBAL CHARACTERISTICS OF ATMOSPHERE EMISSIONS IN THE LOWER THERMOSPHERE AND THEIR AERONOMIC IMPLICATIONS (NASA) 36 p HC $5.00 CSCL 04A G3/13

N74-32784

Unclas
48009

EDITH I. REED
SUSHIL CHANDRA

AUGUST 1974

GSFC
GODDARD SPACE FLIGHT CENTER
GREENBELT, MARYLAND

THE GLOBAL CHARACTERISTICS OF ATMOSPHERIC EMISSIONS IN THE LOWER THERMOSPHERE AND THEIR AERONOMIC IMPLICATIONS

Edith I. Reed and Sushil Chandra

August 1974

NASA GODDARD SPACE FLIGHT CENTER
Greenbelt, Maryland 20771

THE GLOBAL CHARACTERISTICS OF ATMOSPHERIC EMISSIONS IN THE LOWER THERMOSPHERE AND THEIR AERONOMIC IMPLICATIONS

Edith I. Reed and Sushil Chandra
Laboratory for Planetary Atmospheres
Goddard Space Flight Center
Greenbelt, Maryland 20771

ABSTRACT

The green line (557.7 nm) of atomic oxygen and the Herzberg bands of molecular oxygen (measured between 250-280 nm) as observed from the Ogo-4 airglow photometer are discussed in terms of their spatial and temporal distribution and their relation to the atomic oxygen content in the lower thermosphere. Daily maps of the distribution of emissions show considerable structure (cells, patches, and bands) with appreciable changes from day to day. When data are averaged over periods of several days in length, the resulting patterns have only occasional tendencies to follow geomagnetic parallels. The seasonal variation is characterized by maxima in both the northern and southern hemispheres in October, with the northern hemisphere having substantially higher emission rates. These maxima tend to move toward the poles, leaving very low values of emission at low latitudes in December and January. Noting the similarity of the atomic oxygen profiles in the lower thermosphere to that of a Chapman distribution, formulae are derived relating the vertical column emission rates of the green line and the Herzberg bands to the atomic oxygen peak density. Global averages for the time period for these data (August 1967 to January 1968), when converted to maximum atomic oxygen densities near 95 km, have a range of 2.0×10^{11} cm^{-3} to 2.7×10^{11} cm^{-3}. Their variation closely follows the phase of the semi-annual variation in total density observed at higher altitudes from the analysis of satellite drag data.

THE GLOBAL CHARACTERISTICS OF ATMOSPHERIC EMISSIONS IN THE LOWER THERMOSPHERE AND THEIR AERONOMIC IMPLICATIONS

Edith I. Reed and Sushil Chandra

INTRODUCTION

Of the various emissions that originate at altitudes of 85-110 km in the earth's atmosphere, the green line of atomic oxygen (557.7 nm) and the Herzberg bands of molecular oxygen (middle and near ultraviolet) are the most sensitive indicators of the atomic oxygen density in the lower thermosphere.

The green line of atomic oxygen was among the earliest atmospheric emissions to be observed on a regular basis. Analysis of the data from various ground stations indicated a patchy structure with dimensions on the order of hundreds of kilometers and with pronounced spring and fall maxima in average intensities. The altitude of the primary emitting layer was determined by rocket probes to be in the vicinity of 95 km (Offerman and Drescher, 1973, and references therein). The first comprehensive picture of the global distribution of the green line was derived from the Ogo-6 horizon scanning photometer (Donahue et al., 1973). The semi-annual variation of atomic oxygen derived from green line observations assuming the three-body Chapman reaction were found to correspond to the satellite drag semiannual effect. Worldwide maps showed strong variations, with a minimum typically within 15° of the equator and maxima at higher winter latitudes. (Donahue et al., 1974).

Ground observation of the emission rate of the Herzberg bands in the airglow has been hampered by the highly variable transmission of the atmosphere at wavelengths shorter than 400 nm. In fact, from the ground,

the observed Herzberg emissions decrease with increasing zenith angle since atmospheric scattering offsets the increase in emitting path length. Nevertheless, a high correlation between the green line and the Herzberg bands as measured between 300 and 400 nm is usually found (Dick and Sivjee, 1971; Barbier, 1963). From rocket data the Herzberg emissions near 250 nm are found to reach a maximum between 95 and 100 km, and where both are measured simultaneously, the altitude of the Herzberg maximum is close to that of the green line (Reed, 1968; Stecher, 1965; Packer, 1961; Tousey, 1958). The $A^3\Sigma_u^+$ state of molecular oxygen responsible for this emission is one of the products of a three-body collision of atomic oxygen with N_2 or O_2 as the third body.

In this paper we shall present the first comprehensive picture of the Herzberg emissions and discuss their global characteristics in reference to a similar picture deduced from the oxygen green line. By assuming that these emissions are the result of three-body chemiluminiscent reactions, we shall derive analytical expressions relating their column emission rates to atomic oxygen density. These expressions then will be used to derive the global and the seasonal characteristics of atomic oxygen in the lower thermosphere.

INSTRUMENTATION AND DATA REDUCTION

The data for the green line of atomic oxygen and for the Herzberg bands of molecular oxygen were obtained from the main body photometer on the Ogo-4 satellite from mid-August 1967 through the end of January 1968.

The general characteristics of the photometer, the details of its calibration, and the operations of the spacecraft as they affected the

availability of data are given by Reed et al. (1973). Briefly, the main body photometer consisted of eight different mirror positions, six for measurement of the emissions in the various spectral bands in the nadir direction, one for measuring the dark current component, and one for the measurement of 630.0 nm emission in the zenith direction. The two nadir mirror positions of prime interest here are those designated 1 (uv) and 6 (green). Their spectral characteristics are stated in Table 1.

The data reduction proceeded in several steps. First, most of the playback data (from tape recorders on board the spacecraft) were processed to yield a set of tapes giving time, a number indicating the response of the photometer after correction for background emissions, and the location of the point in latitude and longitude. The background for the green line emission of the $O(^1S)$ was obtained by multiplying the response from mirror position 4 (623 nm) by a constant which had been estimated from consideration of the airglow spectrum as published by Broadfoot and Kendall (1968), the spectrum of starlight and zodiacal light, and a nominal earth albedo of 0.4. These data were then smoothed and plotted on microfilm; contour maps of the Herzberg emissions based on these plots are found in Plate 1.

The second step in data reduction was for the purpose of obtaining a world-wide picture of the airglow emissions over the entire time period for which data were available. Averages were made over 5° latitude intervals. All data for which the dark current was greater than the value of the uv signal were deleted (primarily near the South Atlantic magnetic anomaly). To exclude data from aurora, twilight, or moonlit conditions, all data for which the signal from mirror position 7 (391.4 nm) was greater than 40 R were deleted. The F-region component of the $O(^1S)$ green line was assumed

	Wavelength (nm) at stated relative responsivity									
Responsivity	0.01	0.1	0.5	1.0	0.5	0.1	0.01	Effective bandpass	Conversion factors	
Mirror position									continuum	line
1	225.0	243.6	255.4	265.2	277.8	292.0	311.8	25.8	6.175	
2	624.05	626.7	628.45	630.3	631.95	633.62	636.4	4.0	47.4	195.4
3	623.85	626.23	627.90	629.85	631.95	633.45	636.05	4.4	22.6	99.0
4	613.95	617.97	620.17	622.95	625.70	627.97	632.07	5.9	16.26	
5	581.88	584.60	586.40	588.50	590.55	592.17	595.17	4.5	16.08	75.8
6	548.7	552.68	554.90	557.40	560.02	562.55	567.0	5.7	8.93	51.3
7	384.75	388.10	390.02	392.45	394.62	396.50	399.7	4.9	8.54	49.3

Table 1. Response of the airglow photometer. The conversion factors are in Rayleighs per nm per volt for continuum and in Rayleighs per volt for line emissions. The conversion factor for any given time after launch is obtained by multiplying the above conversion factors by $\exp(-1.48\times10^{-3}\ N + 2.22\times10^{-2})$ where N is the number of days and is equal to 1 on January 1, 1967.

to be equal to 1/4 the value of the 630.0 nm emission of $O(^1D)$ and was subtracted from the green line observations.

Finally, the data were divided into 26 groups, each of which contained data for a period of several days, on the basis of whether the orbits were entirely in twilight, the dark side of the earth was moonlit, partially moonlit, or free from moonlight. Zonal averages (all data for each period in each 5° latitude interval) were made and form the basis of Plate 2. It was noted that except when the moon was within 4° of zenith (and moonlight entered the photometer through the zenith port) the contribution of moonlight to the uv data was negligible. This permitted inclusion of the moonlit uv data for mid and low latitudes in the map of the Herzberg band emissions shown in Plate 2.

It is believed that the absolute value of the responsivity of the photometer for visual wavelengths is known to an accuracy of $\pm$ 7%. The systematic and random errors introduced by neglect of temperature changes, neglect of cross-talk contributions, and noise are judged to be generally less than $\pm$ 15% in the data presented here. The inflight calibrations for the visual channels involved several techniques: the observations of stars, incandescent calibration lamps, and comparison with observations from ground observatories. None of these applied to the uv channel, and the data analysis has been done assuming that the responsivity in the uv channel maintained the same fixed ratio to the other channels as it had during the laboratory calibrations.

Most of the uv data are presented in terms of rayleighs/10 nm, which represents the emission rate of a flat continuum in the 250-280 nm wavelength range. Assuming that the Herzberg band emission is that described by Degen (1972), this unit may be converted to total Herzberg band emission by multiplying by 14.7.

Nadir measurements of the 557.7 nm emissions, unlike the uv observations, tend to be increased over areas of high albedo (cloud and snow cover), so that on the average, the values shown are 30 to 40% greater than the actual column emission rates. (For a discussion of albedo in terms of bidirectional reflectance observed from Ogo-4 see Fowler et al.,1971). Short transients due to lightning and energetic particles were minimized by using only the lowest third of the several readings received each second. Cities with much incandescent lighting and areas with many natural gas flares (oil fields and refineries) produce a large signal in the 622.5 nm mirror position, and appear as low values of 557.7 nm emission after the background correction is made. Such areas cover only a small percentage of the earth's surface and were confined principally to industrial parts of Europe and the United States, and to the Middle East.

SPATIAL AND TEMPORAL DISTRIBUTION OF AIRGLOW

Most of the maps presented here are based on the Herzberg emissions as observed from Ogo-4 in the middle ultraviolet. Since the lower atmosphere is opaque in the 250-280 nm region, there is no problem regarding variation of earth albedo due to cloud and snow cover, or with respect to spurious emission sources such as city lights. Neither do we need to take into account an F-region contribution such as is present for the green line.

Daily Maps

Data representative of each of the five moonlight-free periods observed from Ogo-4 are shown in Plate 1. These maps show not only the

Herzberg bands but also the the auroral zone, the Vegard-Kaplan bands of N_2, and, toward the poleward edges of the sunlit (hatched) areas, emission due to rayleigh-scattered sunlight and nitric oxide fluorescence.

All of the maps are characterized by irregular structure, possibly superimposed on a more general pattern similar to those presented by Donahue et al. (1974). The patches are of all shapes and sizes. They tend to form, move around, and disappear over a period of a week or so. In October, there is a large region of high emission at mid-latitudes. There is often a persistent region of enhancement extending toward low latitudes from the auroral region, and moving in longitude over a period of days. In late December and January, there is a minimum at low latitudes extending to as much as 40° on either side of the equator. The maps for the green line emissions show similar features at similar locations.

These patches are considered to be analogous to the green line cells and patches that have been noted by various observers, patches which are characterized by dimensions ranging from 900 to 3000 km, being larger in size in autumn than in winter [Christoffe-Glaume, 1965; Morozov, 1965; Silverman, 1969; Battaner and Pardo, 1972; Neo and Shepherd, 1972].

Average Maps

In order to look for a fixed underlying pattern in the presence of the considerable fluctuations associated with the airglow cells, one can average data over a period of time so as to decrease the effects of the randomly moving structures.

The maps in Figure 1 are the result of such an effort. Auroral and twilight data were discarded by ignoring data when the emission for mirror position 7 (391.4 nm) was greater than 40 rayleighs. The remaining data were averaged over intervals of 5° latitude by 60° longitude, plotted on a map, and appropriate contour lines were drawn. For the sake of continuity, two moonlit maps are included; for these one must ignore the data at auroral latitudes.

The first eight maps in Figure 1 show the development of the autumn maximum. A zone of enhancement, initially at tropical latitudes, intensifies as it moves north. The zone is irregular, clearly influenced by the patchiness characteristic of the daily maps. From a study of the north/south ratios of green emissions observed at several airglow stations, Christoffe-Glaume (1965) suggested that there was a zone of enhanced green line emission parallel to dip latitudes. For the Ogo-4 data, there are only occasional and perhaps fortuitous tendencies for the Herzberg emission contours to follow dip latitudes.

The remaining four maps show the development of the low latitude minimum characteristic of the solstice. The zones of enhanced emission are found only at high latitudes, and the remaining trough does exhibit some tendency to follow magnetic parallels, particularly on the map of December 29. However, this pattern does not persist, and by the end of January, the emission contours appear to be completely unaffected by the magnetic field. The pattern on December 29 could be fortuitous, it could represent some magnetically controlled factor which influences atomic oxygen densities and/or temperatures near 100 km, such as Joule

heating, or it could reflect the behavior at high altitude of a major stratospheric warming which was taking place over Europe and North America.

Seasonal Maps

Data at all longitudes were averaged for the display of the seasonal variations of the Herzberg and green line emissions shown in Plate 2. For these maps, auroral and twilight data were deleted; moonlit ultraviolet data were included.

The resulting averages were plotted as a function of day of year. Early morning data were obtained in late August and December; midnight data in early October and late January, and evening data in late October-November. Simple inspection shows that the latitude distributions for early morning to midnight data in September are quite different from the latitude distributions for the same local times in December-January. Furthermore, observations from ground stations indicate that the diurnal variations are quite variable with altitude and season, and generally have an amplitude of less than 50% (Brenton and Silverman, 1970). Hence the major features of the distribution in Plate 2 are attributed to seasonal effects.

The map of the green line is consistent with the ground observed seasonal variation typical of mid latitude stations, namely, a large autumn maximum, a lesser spring maximum, and a ratio of maximum to minimum of about 3 (Roach et al., 1969).

The principal feature here is one which also was found in the maps of Figure 1, namely that in late summer, an enhancement developed at low

latitudes and rapidly intensified and moved toward the winter pole. In the spring hemisphere, a midlatitude maximum was present throughout the season, without much regular variation, and virtually disappeared (or moved poleward) by midsummer.

Global Averages

To examine long term variations on a world wide basis, "global averages" ($=\Sigma I \cos \lambda$) over the range of latitude (λ) of the Ogo-4 airglow observations were computed for the green line and the Herzberg bands over the various time periods and plotted in Figure 2. The obvious variation here is a semiannual variation with a maximum shortly after equinox and a minimum at solstice.

The average value for the green line data during the whole period of observation is about 150 rayleighs. Assuming an average earth albedo of 35%, this corresponds to a column emission rate of 110 rayleighs. This is somewhat lower than the averages of earlier observations which are in the range of 170 to 260 rayleighs (Petit et al., 1954; Yao, 1962; Hernandez and Silverman, 1964; Roach et al., 1969) but greater than the average observed by Donahue et al. (1973) of about 25 rayleighs.

RELATIONS BETWEEN THE COLUMN EMISSION RATES AND ATOMIC OXYGEN CONCENTRATION

The column emission rates of the green line of atomic oxygen ($O(^1D) - O(^1S)$) and the Herzberg bands of O_2 ($X^3\Sigma_g^- - A^3\Sigma_u^+$) can be directly related to atomic oxygen density which is primarily responsible for these emissions in the lower thermosphere. The derivations of the expressions relating the column emission rates to atomic oxygen are

relatively straight forward if we assume that the chemiluminescent reactions involving these emissions are the result of three-body collisions. Denoting the volume emission rates for green line and Herzberg band emissions by Q_G and Q_H respectively, we may write

$$Q_G = \frac{k_G [O]^3}{1 + (\sum_i q_{Gi} [M_i]/A_G)} \quad (1)$$

and

$$Q_H = \frac{k_H [O]^2 [M]}{1 + (\sum_i q_{Hi} [M_i]/A_H)} \quad (2)$$

where A_G and A_H are the transition probabilities, q_i the quenching coefficient corresponding to the neutral species M_i (N_2, O_2, and O) and [M] the third body. The symbols k_G and k_H are respectively the rate coefficients corresponding to the following reactions

$$O(^3P) + O(^3P) + O(^3P) \rightarrow O_2 + O(^1S) \quad (3)$$

$$O(^3P) + O(^3P) + M \rightarrow O_2 (A^3\Sigma_u^+) + M \quad (4)$$

In the lower thermosphere, the atomic oxygen density distribution is controlled by photochemical and transport processes and must be determined by solving appropriate continuity, momentum, and heat balance equations (Sinha and Chandra, 1974, and the references therein). Denoting the molecular and eddy diffusion coefficients by D and K respectively, we may write

$$[O]_z = [O]_z^o \exp - \int_{z_o}^{z} \frac{v(z)}{D(z) + K(z)} \, dz \quad (5)$$

where

$$[O]_z^o = [O]_{z_o} \exp\left\{-\left[\int_{T_o}^{T} 1 + \frac{D(z)\ K(z)}{D(z) + K(z)}\ \frac{dT}{T} + \int_{z_o}^{z} \frac{]}{D(z) + K(z)}\left(\frac{D(z)}{H(O)} + \frac{K(z)}{H}\right) dz\right]\right\} \quad (6)$$

and v is the velocity which is determined by solving the continuity equation of atomic oxygen:

$$v(z) = \frac{1}{[O]_z} \int_{z_o}^{z} \left(\frac{\partial [O]}{\partial t} - Q - L\right) dz \quad (7)$$

For the purpose of evaluating column emission rate, we find it more convenient to represent equation (5) by a simple analytical expression which can lend itself to an integrable form. Recognizing certain similarities between the O distribution in the lower thermosphere (85-110 km) and the electron density distribution in the F-region, we have chosen the following form analogous to a Chapman distribution:

$$[O]_z = [O]_m \exp \frac{1}{2}\left[1 - \frac{z-z_m}{SH} - \exp\frac{-(z-z_m)}{SH}\right] \quad (8)$$

where $[O]_m$ and z_m are respectively the maximum density and the altitude of the maximum, H the scale height of the mixed atmosphere (tacitly assumed to be that of N_2), and S a scale factor. Whereas both $[O]_m$ and z_m are complex functions of photochemical and transport processes, the physical interpretation of the scale factor S is relatively more apparent. In the altitude region well above the peak, the O concentration according to equation (8) varies as $\exp -(z-z_m)/(2SH)$. If in this altitude region the diffusive separation of the various constituents becomes complete, then $2S \simeq 1.75$, that is, equal to $H(O)/H(N_2)$. However, if the atmosphere is completely mixed then $2S \simeq 1.0$. The scale factor S may, therefore, be interpreted as a parameter reflecting the relative importance of mixing and diffusion in the lower thermosphere. We have attempted to test the validity of equation (8) by fitting it to several theoretical

and measured profiles. By suitable choice of the parameters $[O]_m$, z_m, S, and H, we have been able to get a reasonable fit in most of the cases. For example, with $[O]_m = 1.48 \times 10^{12}$ cm^{-3}, $z_m = 95.2$ km, H = 5.41 km (scale height of N_2 with a temperature of 182°K), and 2S = 1.38, the O concentration as calculated from equation (8) is within 3% of Jacchia 1971 model between 90 and 106 km. At higher altitudes, the departure becomes marked because the underlying assumption of constant temperature no longer holds. This, however, does not cause any serious error in calculating the column emission rate since it is strongly weighted by the O density in the vicinity of the peak. For calculating the column emission rates of the green line, we may adopt the following values for A_G, k_G, and q_{Gi}:

$A_G = 1.24$ sec^{-1}

$k_G = 4.8 \times 10^{33}$ cm^6 sec^{-1} at 300°K (Felder and Young, 1972)

or $k_G = 2.7 \times 10^{-34} \exp(790/T)$ $cm^6 sec^{-1}$ (Donahue et al., 1973)

$q_{G,O} = 7.5 \times 10^{-12}$ $cm^3 sec^{-1}$ at 300°K (Felder and Young, 1972)

or $q_{G,O} = 1.2 \times 10^{-11} \exp(-226/T)$ $cm^3 sec^{-1}$ (Slanger and Black, 1973)

$q_{G,O_2} = 4.3 \times 10^{-12} \exp(-853/T)$ cm^3 sec^{-1} (Slanger and Black, 1973)

$q_{G,N_2} < 5 \times 10^{-17}$ $cm^3 sec^{-1}$ (Atkinson and Welge, 1972)

If we adopt the neutral atmosphere model as given by Jacchia (1971), it is evident that in the lower thermosphere (85-110 km) the only significant quenching is due to atomic oxygen. The expression for I_G, therefore, becomes somewhat simpler as follows:

$$I_G = k_G \int_o^\infty \frac{[O]^3}{1 + q_{G,O}[O]/A_G} \qquad (9)$$

In the two extreme cases when the quenching term is zero or when quenching is large compared to 1, the expressions for I_G with [O] as given by equation (8) are as follows:

$$I_G = 0.1\ e\ A \left(\frac{K_G}{q_{G,O}}\right) S\ H\ [O]_m^2 \quad \text{rayleighs (dominant quenching)} \qquad (10)$$

$$I_G = 0.1\ k_G \left(\frac{2}{3}\ e\right)^{3/2} \Gamma\left(\frac{3}{2}\right) S\ H\ [O]_m^3 \quad \text{rayleighs (no quenching)} \qquad (11)$$

For the intermediate range of quenching values, the integral in equation (9) cannot be integrated in a closed form and must be evaluated numerically. The numerical result may however be expressed in a closed form to a very good degree of approximation as follows:

$$I_G = 0.216 \frac{k_G\ S\ H\ [O]_m^3}{1 + 0.8\ q_{G,O}[O]_m/A_G} \quad \text{rayleighs} \qquad (12)$$

The form of the equation has been chosen to correspond to equations (10) and (11) in the extreme limits of no quenching to dominant quenching.

The relation between I_G and $[O]_m$ as given by equation (12) is shown in Figure 3 using the temperature dependent rate coefficient given earlier in this section. The figure contains two curves with T = 200°K and T=300°K. For comparison, we have also shown the empirical relation between I_G and $[O]_m$ obtained by Donahue et al.(1973), which seems to be in good agreement with our calculated values for T=200°K. If we assume that the altitude of maximum O density is at about 95 km as indicated by the Ogo-6 measurements (Donahue et al., 1973), Figure 3 enables us to estimate the range of variability of atomic oxygen in this altitude region during the observation period of Ogo-4. The global average of 557.7 nm changed from about 160

rayleighs during October 1967 to about 70 rayleighs during January 1968, assuming an albedo of 35%). This would imply a change in O concentration from about 2.7×10^{11} to 2×10^{11} cm^{-3} during this period, provided the product of S and H did not change substantially. The value of atomic oxygen is thus at least a factor of five less than the value indicated by Jacchia's model. This conclusion was also arrived at by Donahue et al (1973) using OGO-6 measurements.

THE COLUMN EMISSION RATE OF THE HERZBERG BAND

Estimating the column emission rate of the Herzberg bands from the neutral composition measurement is much more difficult because of considerable uncertainty in both the rate and the quenching term in equation (2). Since the third body in reaction (4) is either O_2 or N_2, and since N_2 is the major constituent in the lower thermosphere, we may assume that the major contribution to the Herzberg emission comes through the three-body recombination involving N_2 as a third body. This assumption appears to be reasonable since the reaction rates involving O_2 or N_2 as a third body are about equal (McNeal and Durana, 1969, Young and Black 1966). Assuming the N_2 distribution to be in hydrostatic balance, we may write

$$[N_2]_z = [N_2]_m \quad \exp \frac{-(z-z_m)}{H} \tag{13}$$

where $[N_2]_m$ is the density of molecular nitrogen at the altitude, z_m, of the atomic oxygen maximum. With the assumptions outlined above, we may obtain an expression for the column emission rate I_H for the Herzberg bands from equations (2) and (8) as follows:

$$I_H = \int_o^\infty Q_H \, dz$$

$$= 0.1 \, e \, k_H \, S \, H \, [O]_m^2 \, [N_2]_m \quad \Gamma \, (1+S) \qquad (14)$$

For the possible range of S (0.5 to 0.875), Γ (1+S) ranges from 0.89 to 0.95. Adopting a mean value of 0.92, we may write

$$I_H = 0.25 \, k_H \, S \, H \, [O]_m^2 \, [N_2]_m \qquad \text{rayleighs} \qquad (15)$$

The altitude of the maximum emission for the Herzberg bands with respect to the altitude of the maximum emission of the green line may be obtained from the condition $\delta Q_H / \delta z = 0$. It is evident from equation (12) that the maximum emission of the green line occurs at the peak altitude z_m if the quenching is only through atomic oxygen. Denoting by Δz the difference between the peak altitudes of the two emissions, we may write

$$\Delta z = - S \, H \, \ln (1+S) \qquad (16)$$

With H = 5.41 km and S = 0.69, as deduced from the Jacchia 1971 model, the Herzberg peak according to equation (16) is 2.0 km below the greer emission peak. Since the peak altitude of the green emission is near 97 km (Donahue et al 1973), it is evident from equation (16) that the Herzberg emission originates from the same altitude region, a conclusion in basic agreement with the rocket results of Packer (1961).

Equation (15) enables us to estimate the reaction rate k_H of the three-body recombination giving Herzberg emissions.

If we adopt values of $[N_2]_m = 1.85 \times 10^{13}$ cm^{-3}, $[O]_m = 1.5 \times 10^{12}$ cm^{-3}, H = 5.41 km, and S = 0.69, in accordance with the Jacchia 1971 model, then the value of k_H using a global value of I_H = 550 rayleighs is

1.4×10^{-35} cm^6 sec^{-1}. This is almost three orders of magnitude less than 9.6×10^{-33} cm^6 sec^{-1}, the three-body reaction rate given by Campbell and Thrush (1967) at 200°K. If we accept both these rates as approximately correct, it would imply that only 0.14 percent of the molecules are produced in the $A^3\Sigma_u^+$ state in the three-body reaction. On the other hand, if the atomic oxygen density is 2.7×10^{11} cm^{-3} (as implied by the 557.7 nm measurements) then the reaction rate inferred for the formation of the $A^3\Sigma_u^+$ state from the Herzberg measurement is 5 percent of the value deduced by Campbell and Thrush and in general agreement with a similar inference by Sharp and Rees (1970).

CORRELATION BETWEEN THE COLUMN EMISSION RATES--HERZBERG BANDS AND GREEN LINE

A certain degree of correlation between the column emission rates of the Herzberg bands and the green line is to be expected since both of them are proportional to atomic oxygen to a varying degree. From equations (12) and (15), we may write

$$\frac{I_H}{I_G} = \frac{k_H}{k_G}\left(1 + 0.8\ (q_{G,O} / A_G)\ [O]_m\right)\frac{[N_2]_m}{[O]_m} \qquad (17)$$

If the quenching term in equation (12) is dominant, equation (17) is reduced to the following form:

$$\frac{I_H}{I_G} = 0.8\left(\frac{k_H}{k_G}\right)\left(\frac{q_{G,O}}{A_G}\right)[N_2]_m \qquad (18)$$

which indicates that I_H and I_G are linearly related if $[N_2]_m$ does not vary significantly over the range of variability of I_H and I_G. A scatter plot of I_G and I_H is shown in Figure (4). This was made by taking zonal averages (over 5° latitude intervals) of the green line and the Herzberg emissions during September 2-10, 1967. A linear relation between I_G and I_H is quite apparent in this plot. However, the intercept is not zero as would be implied from equation (17).

The plots of I_H and I_G over different periods show basically the same features, with a linear correlation coefficient ranging from 0.8 to 0.95. The average slope of the scatter plot in Fig. (4) is 8 and the zero intercept is -82 rayleighs on the green line axis and 10.2 rayleighs/10nm on the Herzberg emission axis.

The physical significance of the non zero intercept is not quite apparent. Of course if the peak atomic oxygen density is in the range of 2 to 5 x 10^{11} cm^{-3}, as implied by the green emission, then the quenching term in equation (17) is comparable to one and the slope of the scatter plot would vary over a wide range because of the variability in $[O]_m$. This may give an illusion of the non zero intercept in Figure (3). The zero intercept may also be due in part to over correction of the mirror position 6 (green line) data with respect to background and F-region contributions, to changes in filter characteristics, and/or to fluorescence of the front window; although difficult to assess, these factors do not appear to be sufficient to account for the intercept observed. Notwithstanding these uncertainties, a very good correlation between the column emission rates of the Herzberg band and the green line substantially supports the theory of three-body collisions as the source of these emissions and the general validity of equations (12) and (15).

SEMI ANNUAL VARIATION

The global averages of the green line emission found in Figure 2 can be converted to peak atomic oxygen densities by the use of equation

(12). The results, assuming an average earth albedo of 35%, a temperature of 200°K and S = 0.76, have been plotted in Figure 5.

The principal feature of Figure 5 is the semiannual variation. The effects of diurnal variations as exhibited in green line emissions have been shown to be highly variable, dependent on both latitude and season, and to be generally less than 50%, or, in terms of computed atomic oxygen density, less than 7% (Brenton and Silverman 1970). This is but a small fraction of the variation exhibited in Figure 5. Likewise, the effects of lunar tides should be virtually undetectable, being less than 3% in terms of atomic oxygen density (Forbes and Geller 1972). Variations in magnetic activity affect primarily high latitude data (Silverman 1969), little of which is included in these global averages.

It is of interest to compare the variation of $[O]_m$ with the variation of total density at higher altitudes. For this we have used the data derived from the drag analysis on Satellite 1966 44A (Explorer 32), Jacchia 1971 and 1971a. To facilitate comparison of phase, the $\Delta \log \rho$ (fractional variation of density) has been plotted about a nominal value of $2.2 \times 10^{11} cm^{-3}$. With respect to the amplitude of the density variations, it is fortuitous that the effective height of Explorer 32 (about 300 km) happened to be such that the corresponding variation of total density was nearly equal to the variation in the maximum atomic oxygen densities near 97 km. More important is that the phase of the density variations is very similar for both sets of data. Hence one can conclude that the dominant variation in the global average of the maximum atomic oxygen density is similar to the semi annual variation in total density observed at higher altitudes.

CONCLUDING REMARKS

In this paper, we have studied the global characteristics of the column emission rates of the green line (557.7 nm) of atomic oxygen and the Herzberg emissions of the O_2 in the uv range. The observational data for the study was obtained from the Ogo-4 airglow photometer during 1967-68, a period of high solar activity. By attributing these emissions to chemiluminescent reactions involving three-body collisions, we derived simple analytical expressions relating the column emission rates to atomic oxygen density in the lower thermosphere. The atomic oxygen density estimated from the airglow observations has been found at least a factor of five less than the Jacchia 1971 model but in general agreement with the values deduced by Donahue et al. (1973) from the Ogo-6 airglow scanning photometer.

Although the daily maps of airglow are characterized by a patchy, irregular, and changing structure, several conclusions can be reached regarding the general behavior of peak atomic oxygen densities as revealed by airglow emissions:

(1) A region of enhancement developed at low latitudes near equinox (September) and moved toward the winter pole, intensifying with time and reaching the polar region by early November. A lesser enhancement was noted at mid latitudes in the spring hemisphere during the corresponding period. Irregularity of structure and movement were present both within and without the regions of enhancement.

(2) A wide low and midlatitude minimum with boundaries on the order of 35°N and 35°S developed during December and remained through January.

(3) A tendency to follow magnetic parallels appeared in late October and late December. However, irregularities were superimposed, and the appearance of magnetic control may be fortuitous.

(4) When data is averaged in both latitude and longitude (global averages), a marked variation in the peak atomic oxygen densities is seen, similar in phase to that of the density residuals attributed to the semiannual variation in the data from the drag analysis of Explorer 32 for the same time period.

ACKNOWLEDGEMENTS

The data was from the Ogo-4 Airglow Photometer Experiment, for which Professor Jacques E. Blamont of the Centre National de la Recherche Scientifique (France) was co-experimenter. Much of the data reduction was accomplished by Jacques Pacquet, also of CNRS. Walter Fowler, of the Goddard Space Flight Center, contributed the conversion of the uv data to the total emission rate of the Herzberg bands.

REFERENCES

Atkinson, R., and K. H. Welge, Temperature dependence of $O(^1S)$ deactivation by CO, O_2, N_2 and Ar*, J. Chem. Phys., 57, 3689-3693, 1972.

Barbier, D., Introduction a l'étude de la luminescence atmosphérique et de l'aurore polaire, Geophysics, the Earth's Environment, ed. C. DeWitt, J. Hieblot, and A. Lebeau, Gordon and Breach, Science Publ., New York, 1963, pp. 303-368.

Battaner, E. and G. Pardo, Observations on airglow green cells, Ann. Géophys., 28, 731-734, 1972.

Brenton, J. G., and S. M. Silverman, A study of the diurnal variations of the 5577 A (OI) airglow emission at selected IGY stations, Planet. Space Sci., 18, 641-653, 1970.

Broadfoot, A. L., and K. R. Kendall, The airglow spectrum, 3100-10,000 A, J. Geophys. Res., 73, 426-428, 1968.

Campbell, I. M., and B. A. Thrush, The association of oxygen atoms and their combination with nitrogen atoms, Proc. Roy. Soc. London A, 296, 222-232, 1967.

Christophe-Glaume, J., Etude de la raie 5577 A de l'oxygene dans la luminescence atmospherique nocturne, Ann. Géophys., 21, 1-57, 1965.

Degen, V., Vibrational populations of O_2 $(A^3\Sigma_u^+)$ and synthetic spectra of Herzberg bands in the night airglow, J. Geophys. Res., 74, 5145-5154, 1969.

Dick, K. A. and G. G. Sivjee, O_2 Herzberg I bands in the night airglow: covariation of OI (5577), J. Geophys. Res., 76, 6987-6989, 1971.

Donahue, T. M., B. Guenther, and R. J. Thomas, Distribution of atomic oxygen in the upper atmosphere deduced from Ogo 6 airglow observations, J. Geophys. Res., 78, 6662-6689, 1973.

Donahue, T. M., B. Guenther, and R. J. Thomas, Spatial and temporal behavior of atomic oxygen determined by Ogo 6 airglow observations, J. Geophys Res., 79, 1959-1964, 1974.

Felder, W., and R. A. Young, Quenching of $O(^1S)$ by $O(^3P)$*, J. Chem. Phys., 56, 6028-6030, 1972.

Forbes, J. M., and M. A. Geller, Lunar semidiurnal variation in OI (5577 A) nightglow, J. Geophys. Res., 77, 2942-2947, 1972.

Fowler, W. B., E. I. Reed, and J. E. Blamont, Bidirectional reflectance of the moonlit earth, App. Opt., 10, 2657-2660, 1971.

Hernandez, G. J. and S. M. Silverman, A re-examination of Lord Rayleigh's data on the airglow 5577 A(OI) emission, Planet. Sp. Sci., 12, 97-112, 1964.

Jacchia, L. G., Revised static models of the thermosphere and exosphere with empirical temperature profiles, Smithsonian Astrophysical Obs., Special Report 332, 1971.

Jacchia, L. G., Semiannual variation in the Heterosphere: a reappraisal, J. Geophys. Res., 76, 4602-4607, 1971a.

McNeal, R. J., and S. C. Durana, Absolute chemiluminescent reaction rates for emission of the O_2 Herzberg bands in oxygen and oxygen-inert-gas afterglows, J. Chem. Phys., 51, 2955-2960, 1969.

Morozov, V. M., Some space and time characteristics of the [OI] 5577 Å airglow emission. Geomag. Aeron., 5, 224-226, 1965.

Neo, Y. P., and G. G. Shepherd, Airglow observations with a Hadamard photometer, Planet. Space Sci., 20, 1351-1355, 1972.

Offermann, D., and A. Drescher, Atomic oxygen densities in the lower thermosphere as derived from in situ 5577-A night airglow and mass spectrometer measurements, J. Geophys. Res., 78, 6690-6700, 1973.

Packer, D. M., Altitudes of the night airglow radiations, Ann. Géophys., 17, 67-75, 1961.

Pettit, H. B., F. E. Roach, P. St. Amand, and D. R. Williams, A comprehensive study of atomic emissions in the nightglow, Ann. Géophys., 10, 326-347, 1954.

Reed, E. I., A night measurement of mesospheric ozone by observations of ultraviolet airglow, J. Geophys. Res., 73, 2951-2957, 1968.

Reed, E. I., W. B. Fowler, and J. E. Blamont, An atlas of low-latitude 6300-A (OI) night airglow from Ogo 4 observations. J. Geophys. Res., 78, 5658-5675, 1973.

Roach, F. E., L. L. Smith, and J. R. McKennan, Night airglow observations during the IQSY, Ann. IQSY, 4, 375-387, Ed. A. C. Stickland, MIT Press, Cambridge, Mass., 1969,

Sharp, W. E. and M. H. Rees, Latitudinal distribution of night airglow, J. Geophys. Res., 75, 4894-6, 1970.

Silverman, S. M., Night airglow phenomenology, Atmospheric Emissions, Ed. B. M. McCormac and A. Omholt, Van Nostrand Reinhold Co., New York, 383-397, 1969.

Sinha, A. K., and S. Chandra, Seasonal and magnetic storm related changes in the thermosphere induced by eddy mixing, J. Atmos. Terr. Phys., 36, 1974.

Slanger, T. G., and G. Black, O(^{1}S) quenching profile between 75 and 115 km, Planet. Space Sci., 21, 1757-1761, 1973.

Stecher, T. P., The spectral energy distribution of the earth's ultraviolet night airglow, J. Geophys. Res., 70, 2209-2211, 1965.

Tousey, R., Rocket measurements of the night airglow, Ann. Géophys., 14, 186-195, 1958.

Yao, I. G., Observations of the night airglow, Ann. of the IGY, Vol. 24, Pergamon Press, New York, 1962, p. xix.

Young, R. A. and G. Black, Excited-state formation and destruction in mixtures of atomic oxygen and nitrogen, J. Chem. Phys., 44, 3741-3751, 1966.

Plate 1. Ultraviolet emissions observed over 24-hour periods, with color indicative of emission rate. Note that the latitude scale is about 10 times the longitude scale. Local time at the equator is 0242, 0004, 2150, 0219, and 0033 hours for the September through January maps respectively. Date is Universal Time.

Plate 2. The variation of the emission of the Herzberg bands and the green line of atomic oxygen as a function of latitude and day of year. The heavy lin represents the dip equator.

Figure 1. Maps of Herzberg airglow emissions averaged over time periods of several days each. Shading is used to represent high emission rates. Auroral contributions are included in the moonlit maps of Sept. 15 and Dec. 15.

Figure 2. Global averages of the Herzberg band and green line emissions for various periods of observations.

Figure 3. The column emission rate for the green line as related to the peak atomic oxygen density through equation (12) and also by Donahue et al., 1973.

Figure 4. A scatter plot to show the correlation of the Herzberg band emission with the green line emissions. A linear regression analysis for the 1111 points shown here yields $X = 8.0Y - 82.$, where X is the green and Y is the Herzberg emission rate, with a correlation coefficient of 0.90.

Figure 5. Average atomic oxygen densities as derived from the average 557.7 nm emission rates in Figure 2. The solid line is the semiannual density variation as observed from drag analysis on Satellite 1966 44A (Explorer 32) normalized around a value of 2.4×10^{11} cm^{-3} (Jacchia 1971).

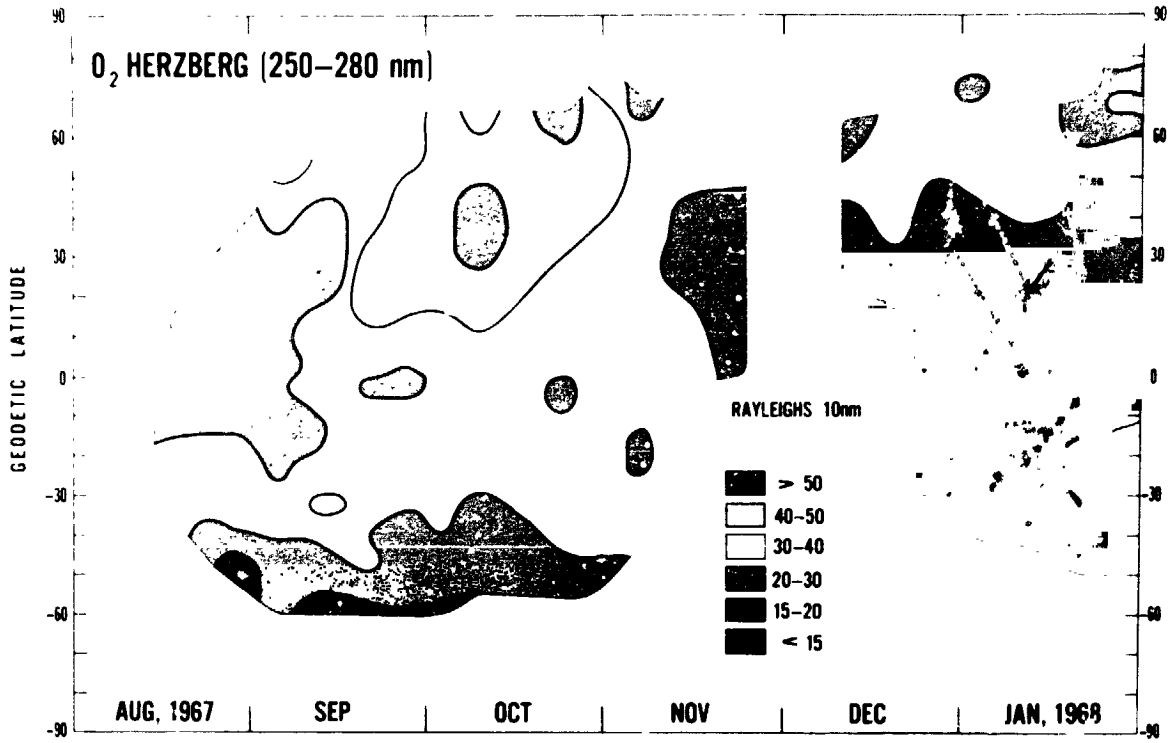

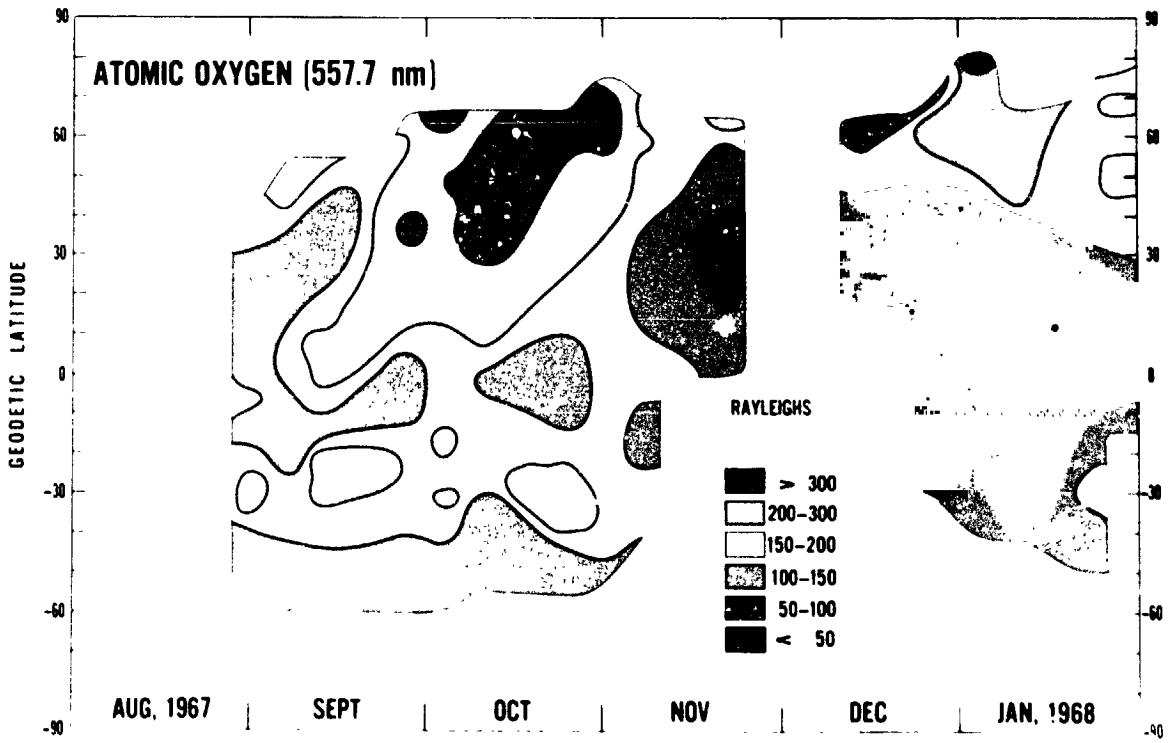

O_2 HERZBERG BANDS (250-280 nm)

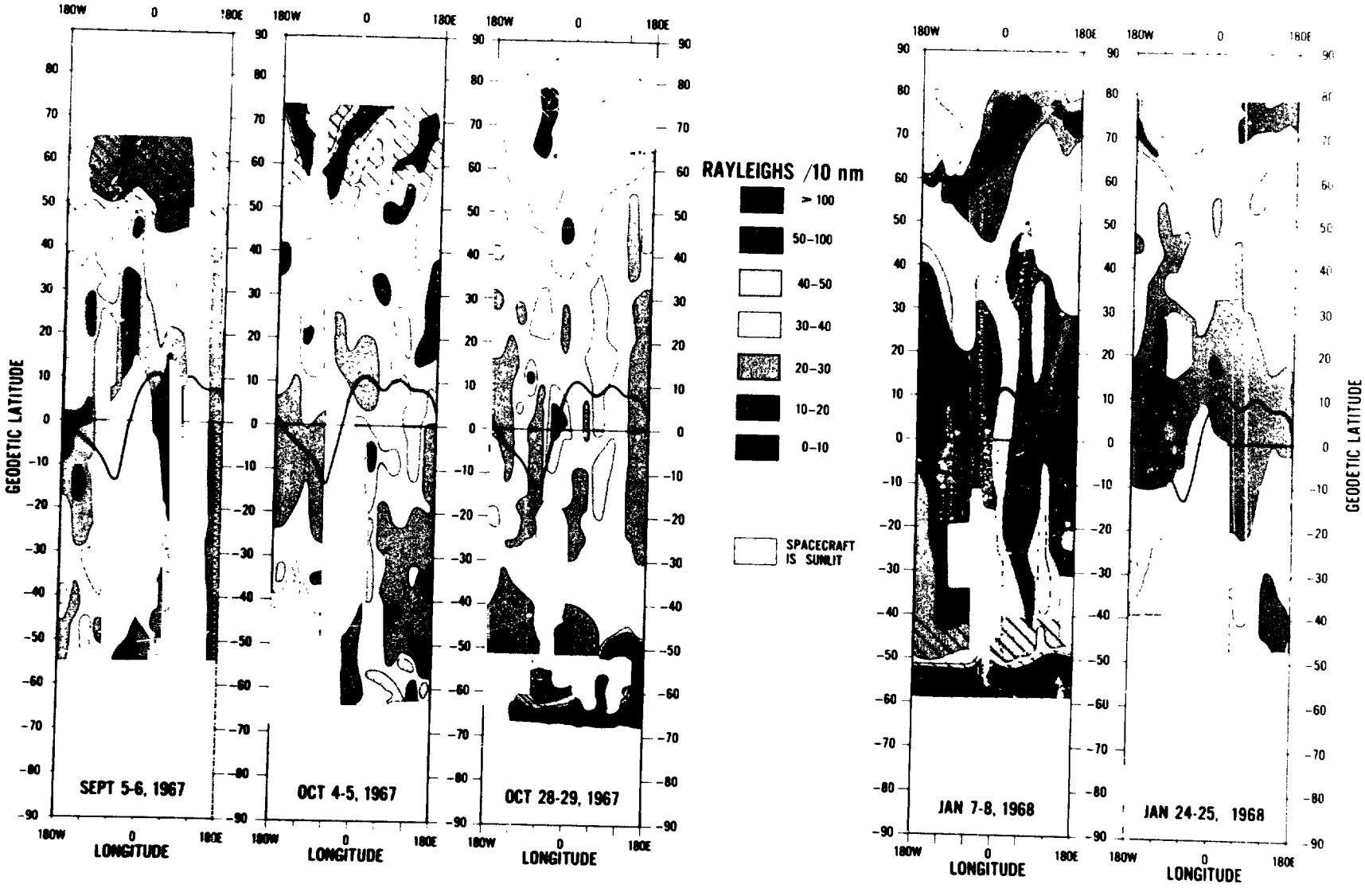

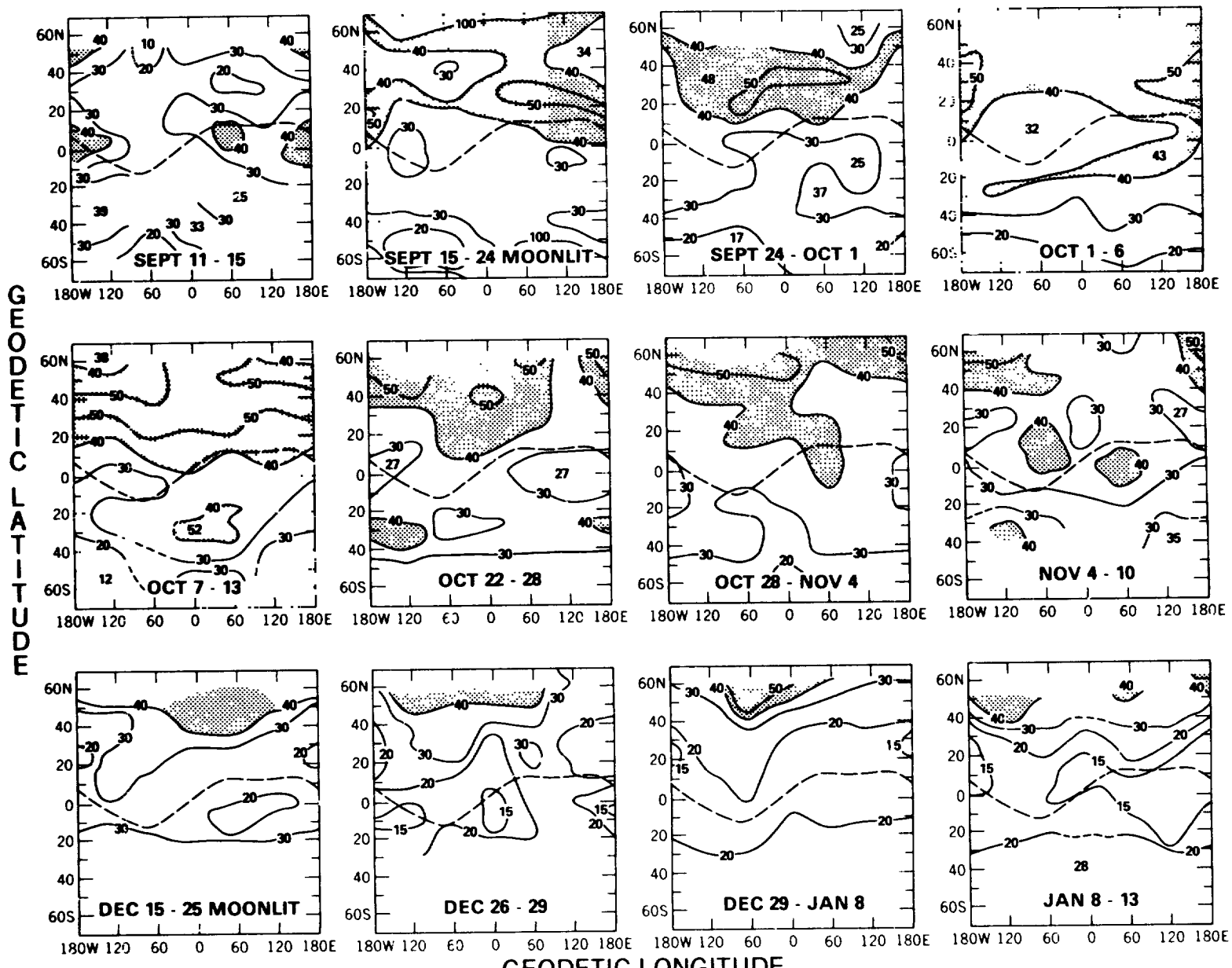
SEPT 11 - 15
SEPT 15 - 24 MOONLIT
SEPT 24 - OCT 1
OCT 1 - 6
OCT 7 - 13
OCT 22 - 28
OCT 28 - NOV 4
NOV 4 - 10
DEC 15 - 25 MOONLIT
DEC 26 - 29
DEC 29 - JAN 8
JAN 8 - 13
60N
60S
180W 120 60 0 60 120 180E
GEODETIC LATITUDE
GEODETIC LONGITUDE
HERZBERG 250 - 280 nm

Fig. 1

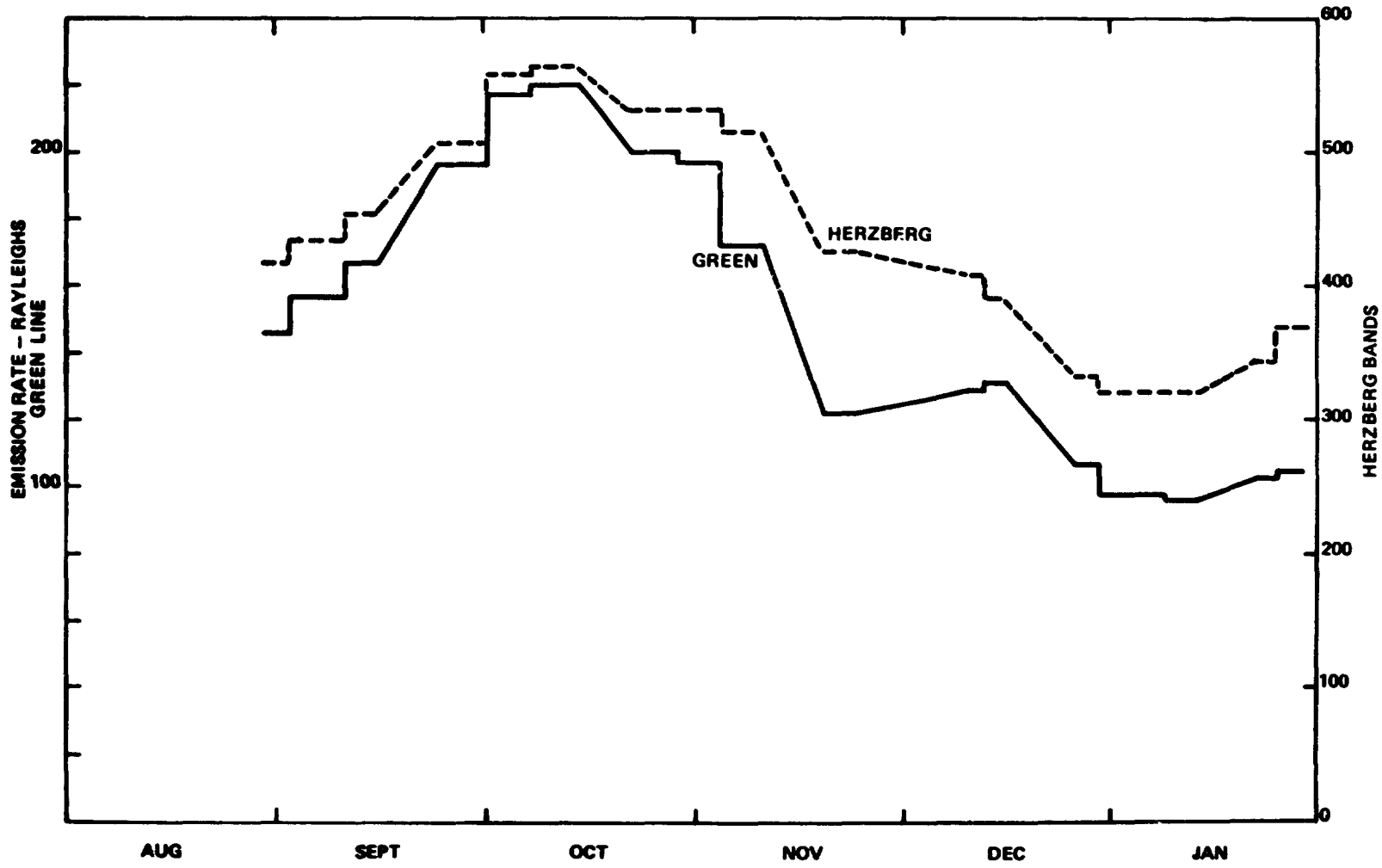
EMISSION RATE – RAYLEIGHS
GREEN LINE
200
100
HERZBERG
GREEN
600
500
400
300
200
100
0
HERZBERG BANDS
AUG
SEPT
OCT
NOV
DEC
JAN

Fig. 2

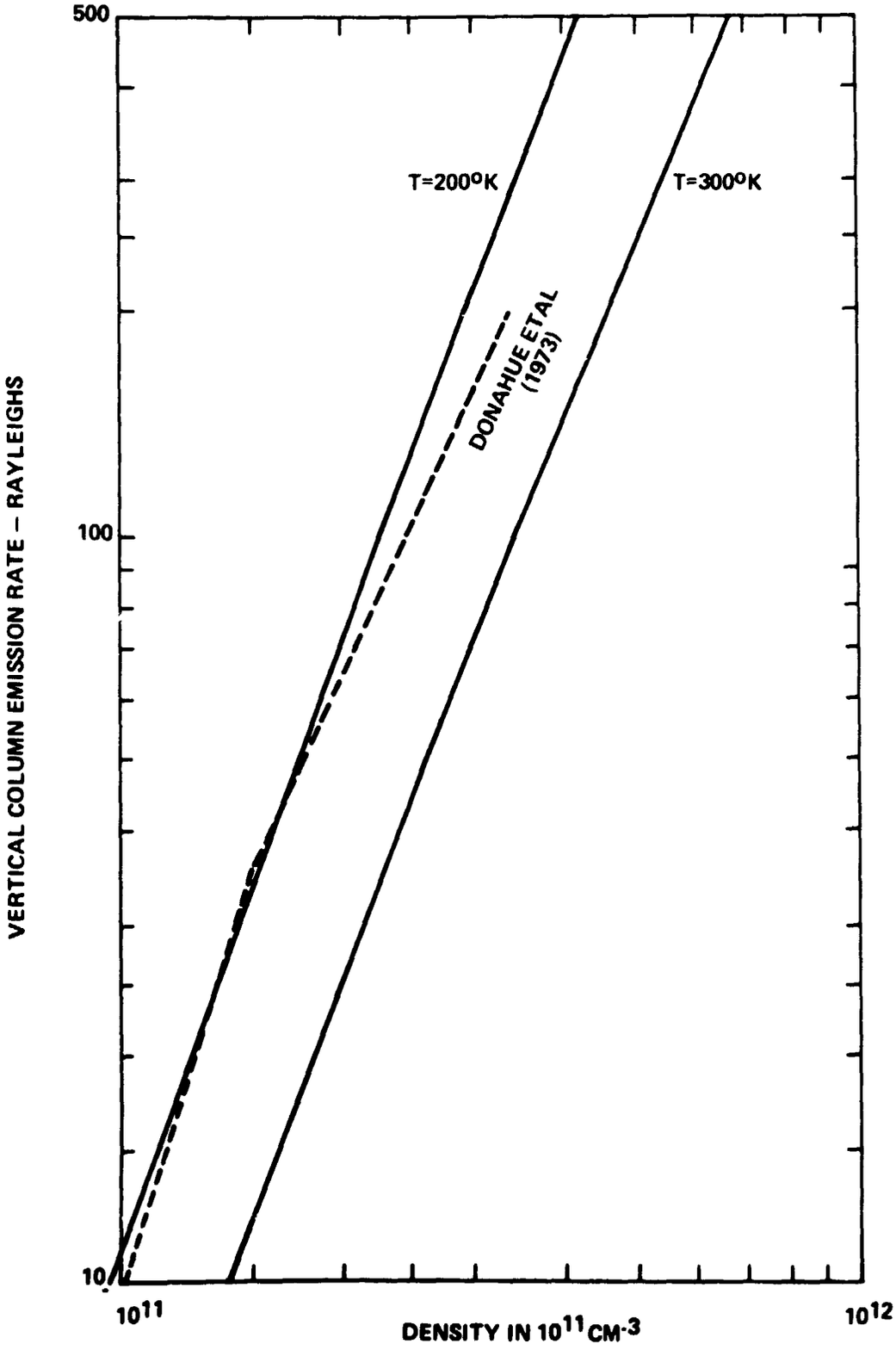
500
100
10
T=200°K
T=300°K
DONAHUE ETAL (1973)
VERTICAL COLUMN EMISSION RATE – RAYLEIGHS
10^{11}
10^{12}
DENSITY IN 10^{11} CM^{-3}

Fig. 3

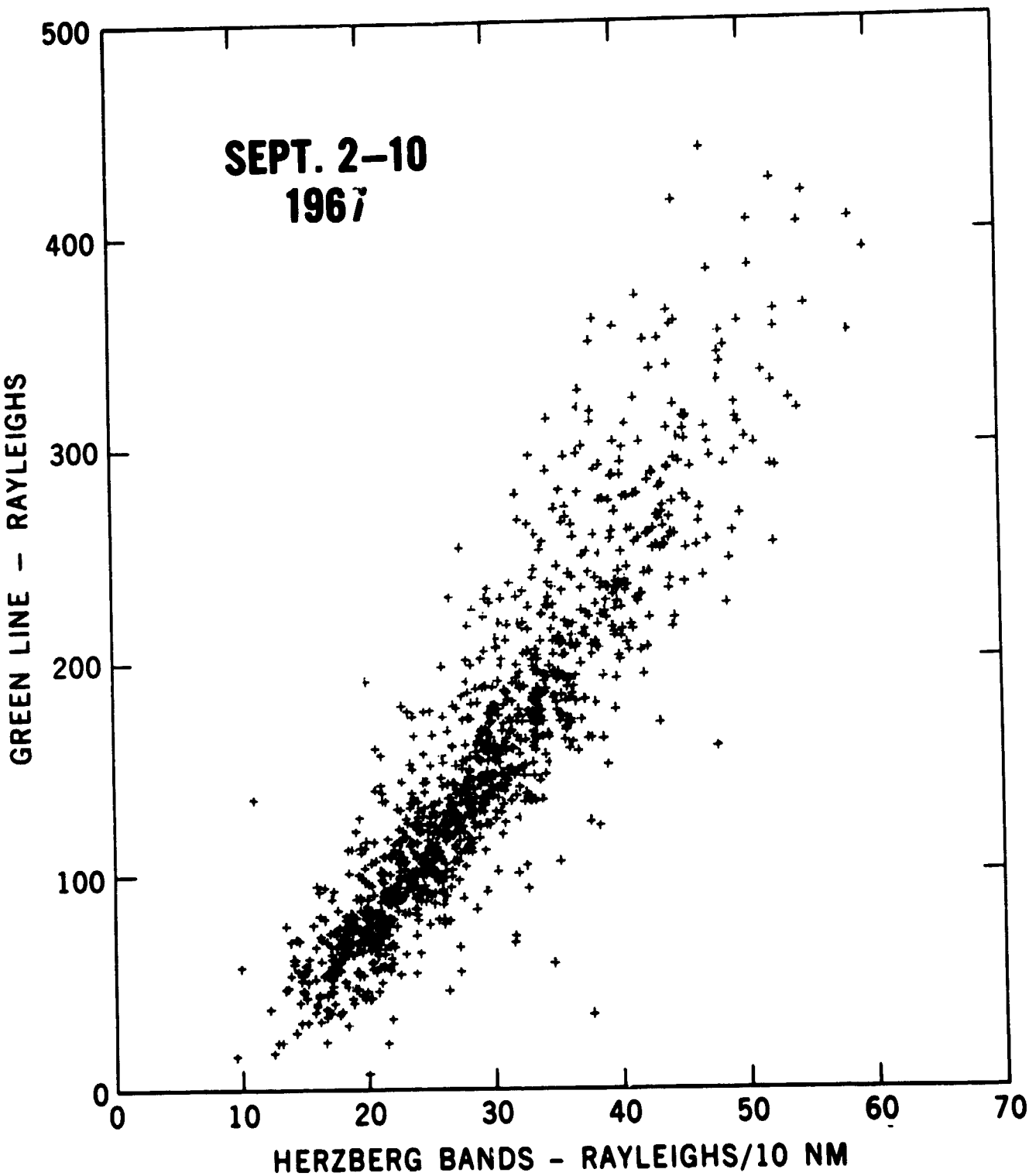

Fig. 4

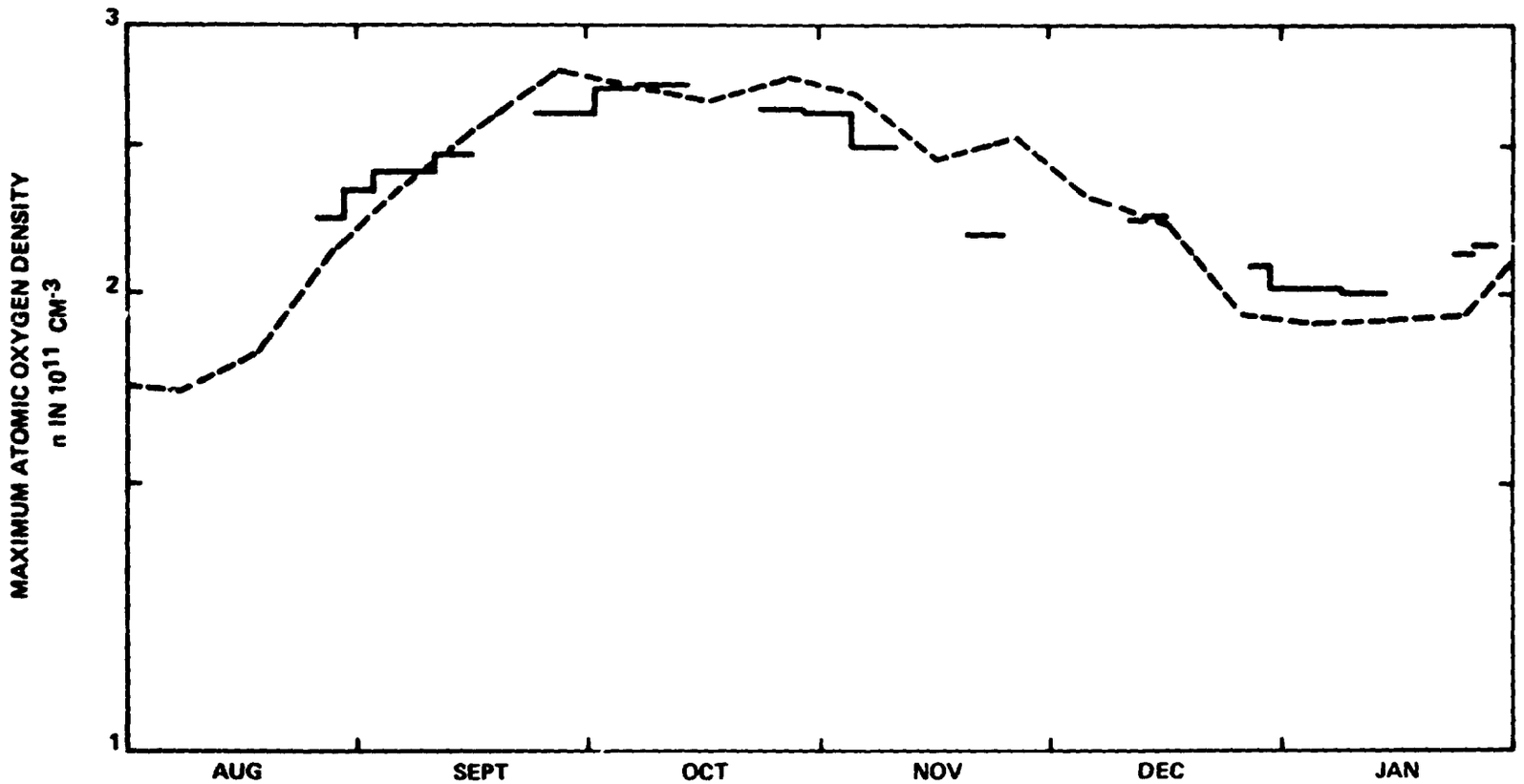
MAXIMUM ATOMIC OXYGEN DENSITY
n IN 10^{11} CM^{-3}
3
2
1
AUG
SEPT
OCT
NOV
DEC
JAN

Fig. 5